Supporting Information

Micron-sized encapsulated-type MoS_2/C hybrid particulates with effective confinement effect for improving cycling performance of LIB anodes

Boya Sun, Qinglei Liu*, Wenshu Chen, Ning Wang, Jiajun Gu, Wang Zhang, Huilan Su, and Di Zhang*

State Key Laboratory of Metal Matrix Composites, Shanghai Jiao Tong University, 800 Dongchuan Road, Shanghai 200240, P. R. China

* liuqinglei@sjtu.edu.cn; zhangdi@sjtu.edu.cn

Figure S1. Digital photographs of cross-linked Mo/SA gels and freeze-dried globules.

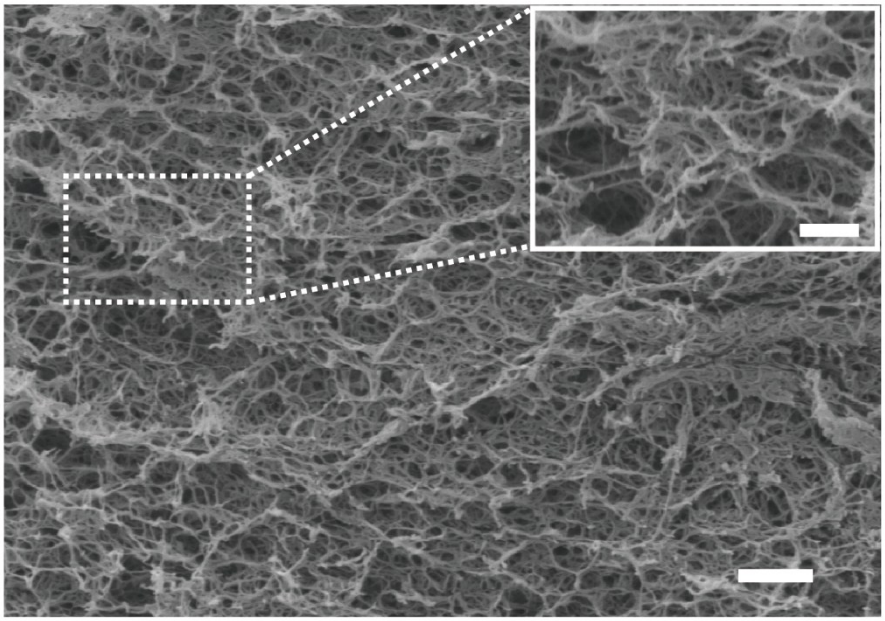

Figure S2. SEM image of Mo/SA gel globules after freeze-dring. Scar bar is 1 μm (500 nm for inset image).

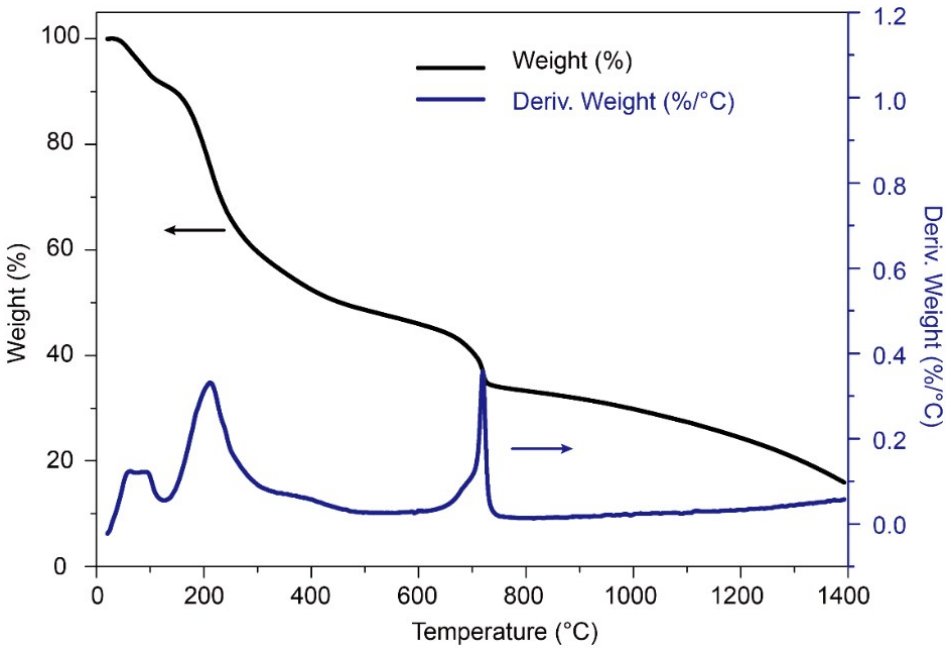

Figure S3. TG curve of Mo/SA gels acquired under a heating rate of 10 ^{o}C min^{-1} in Ar atmosphere.

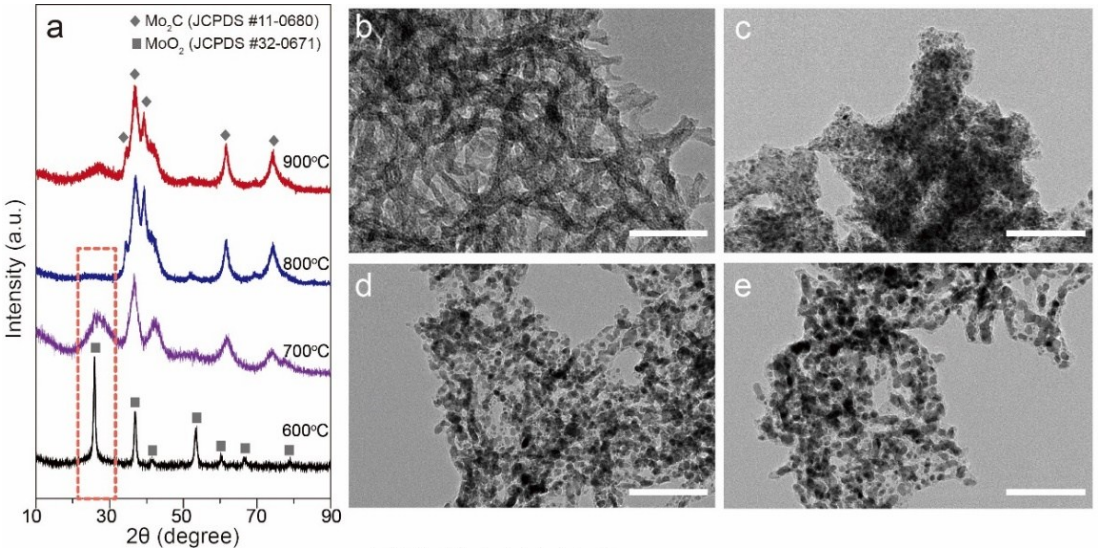

Figure S4. (a) XRD profiles and (b-e) TEM images of the as-synthesized nanocomposites carbonized at 600 ^{o}C (b), 700 ^{o}C (c), 800 ^{o}C (d), and 900 ^{o}C (e), respectively, before sulfurization. The sizes of particles in carbonized samples are 3, 5, 10, and 15 nm, respectively. Scale bars are 100 nm.

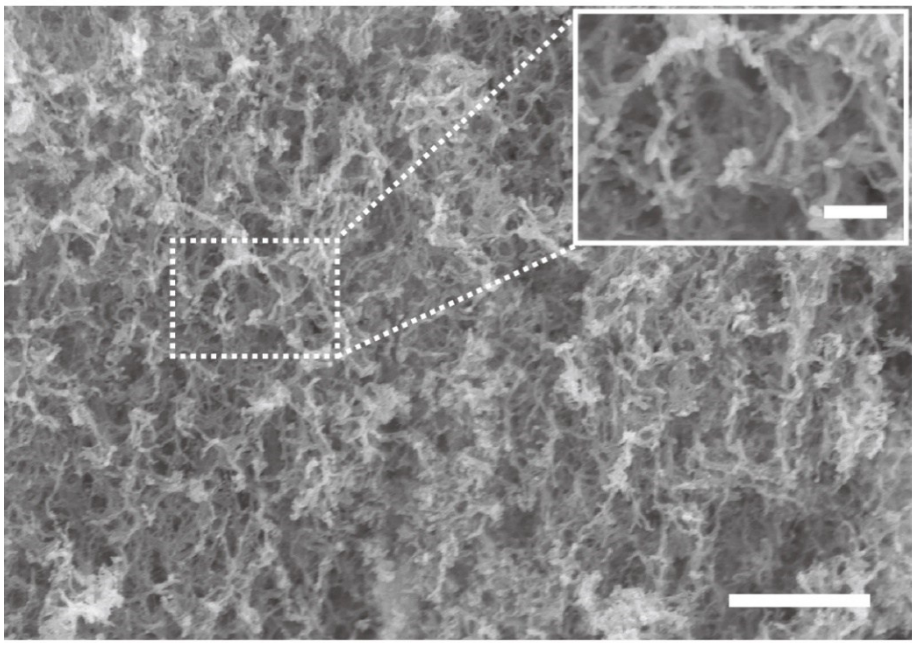

Figure S5. SEM image of Mo_2C/C hybrids after carbonization at 900 °C. Scar bar is 1 μm (200 nm for inset image).

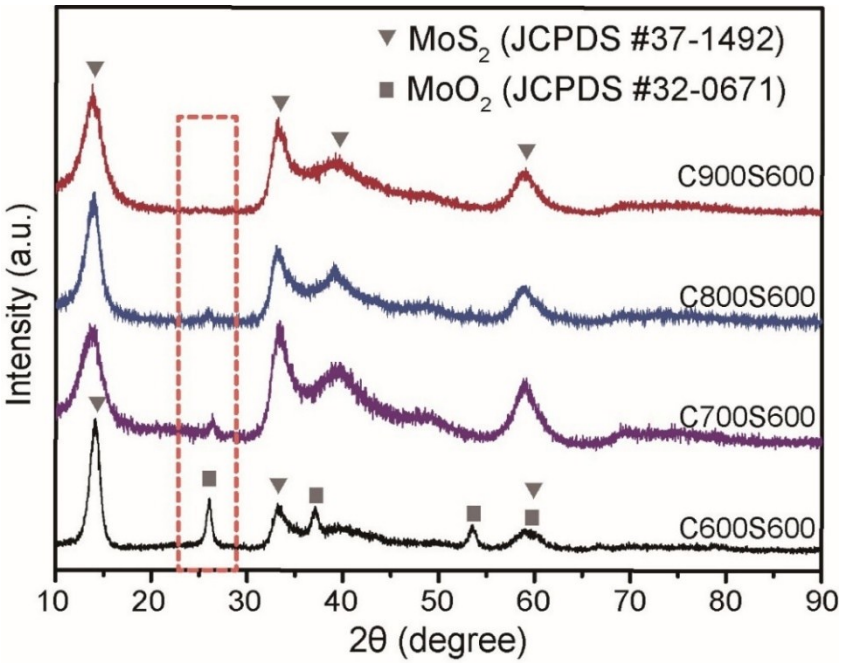

Figure S6. XRD profiles of samples obtained after rapid sulfurization at 600 °C and they are labeled as C600S600, C700S600, C800S600 and C900S600, respectively. For the sulfurized samples, the diffraction peaks of MoO_2 gradually disappear with the increase of initial carbonization temperature. Pure hexagonal MoS_2 phase is obtained in the C900S600 sample (MoS_2/C).

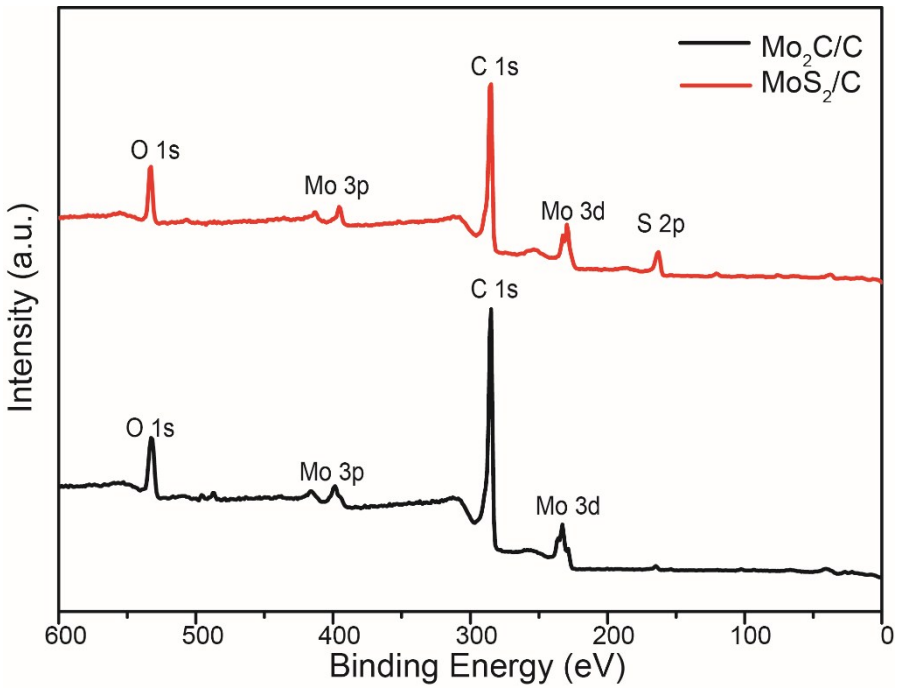

Figure S7. XPS spectra of Mo_2C/C and MoS_2/C hybrids.

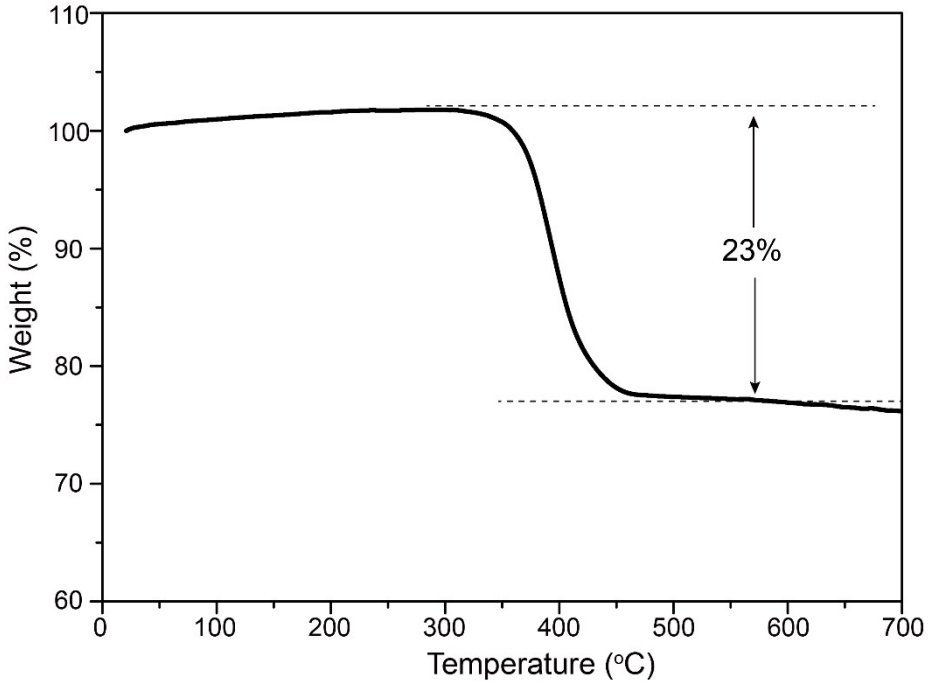

Figure S8. TG curve of MoS_2/C hybrids recorded with a temperature ramp of 10 °C min^{-1} under air atmosphere. The weight loss at about 400 °C comes from the oxidation of MoS_2 to MoO_3. The weight content of MoS_2 in composite is calculated to be 85.6 %.

Table S1. Details of the porous structure characteristics of Mo_2C/C and MoS_2/C hybrids.

	S_{BET} ($m^2\ g^{-1}$)	S_{mi} ($m^2\ g^{-1}$)	S_{me} ($m^2\ g^{-1}$)	V_t ($cm^3\ g^{-1}$)	V_{mi} ($cm^3\ g^{-1}$)	V_{me} ($cm^3\ g^{-1}$)
Mo_2C/C	361.73	192.16	169.57	0.31	0.09	0.22
MoS_2/C	430.72	266.96	163.76	0.38	0.12	0.26

S_{mi}, specific surface area of the micropores; S_{me}, specific surface area of the mesopores; V_t, total pore volume; V_{mi}, pore volume of micropores; V_{me}, pore volume of mesopores.

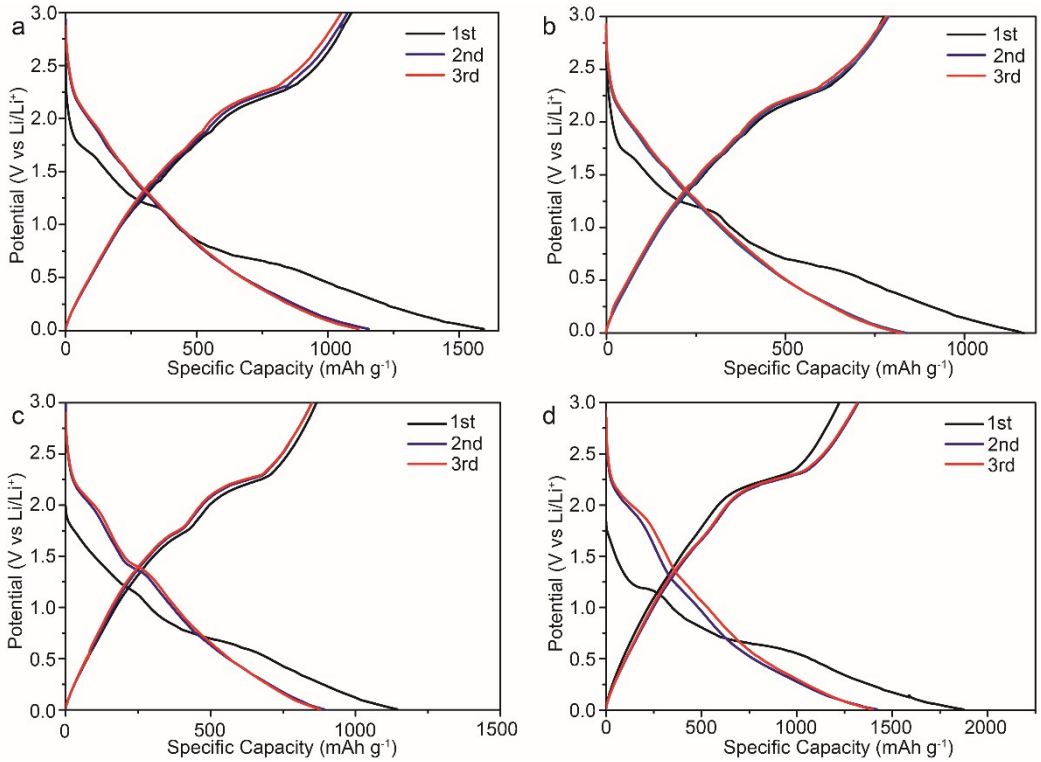

Figure S9. Galvanostatic charge/discharge profiles of (a) C600S600, (b) C700S600, (c) C800S600, and (d) C900S600 (i.e. MoS_2/C) samples during initial three cycles.

Table S2. Summary of LIB properties for MoS_2 based electrodes.

Material	Synthesis method	First discharge capacity (mAh g^{-1})	First charge capacity (mAh g^{-1})	Capacity after (n) cycles (mAh g^{-1})	Coulombic efficiency %	Current density (mAh g^{-1})	Rate capability (mAh g-1) at (X) current density	Ref.
MoS_2/C	**Thermal reaction**	**1873**	**1222**	**1300 (100)**	**97.2**	**100**	**929 (1000 mA g^{-1})**	**this work**
				1250 (480)	**98.5**	**1000**		
MoS_2-amC	Solvethermal	1062	917	907 (50)	98*	1062	700 (53.1 A g^{-1})	1
MoS_2-graphene	Hydrothermal	1571	1031	1187 (100)	—	100	~900 (1000 mA g^{-1})	2
MoS_2-rGO	Exfoliation	1240	—	890 (100)	—	100	600 (1000 mA g^{-1})	3
MoS_2-rGO	Hydrothermal	1367	912	808 (100)	—	100	571 (1000 mA g^{-1})	4
MoS_2-rGO	Hydrothermal	1426	934	1020 (100)	—	100	760 (1000 mA g^{-1})	5
MoS_2-3D graphene	CVD and thermal decomposition	1222	1020	877 (50)	—	100	597 (1000 mA g^{-1})	6
MoS_2-rGO	Exfoliation	971	658	915 (700)	>97	500	339 (20 A g^{-1})	7
MoS_2-rGO	Hydrothermal	1653	1176	1183 (100)	~100	100	901 (1000 mA g^{-1})	8
MoS_2-rGO	Hydrothermal	1592	1036	1063 (100)	100	100	732-718 (1000 mA g^{-1})	9
MoS_2-rGO	Exfoliation	1560	1220	1216 (30)	—	74	711 (1860 mA g^{-1})	10
MoS_2-graphene	Hydrothermal	936	820	1100 (50)	>99	1000	820 (10 A g^{-1})	11
MoS_2-graphene	Exfoliation	1780	1399	1351 (200)	—	100	591 (1000 mA g^{-1})	12
MoS_2-C sheets	Thermal reaction	1654	1161	~1127 (200)	~100	100	250 (10 A g^{-1})	13
MoS_2-SiO_2-graphene	Hydrothermal	1266	1019	1060 (100)	—	100	580 (8 A g^{-1})	14
MoS_2@GF/CNT	Hydrothermal	1568	1252	1112 (120)	81.3	200	823 (5 A g^{-1})	15
MoS_2-graphene	Hydrothermal	1521	1110	1150 (60)	—	100	890 (1000 mA g^{-1})	16
MoS_2-CNT	Microwave	1280	790	927* (80)	96*	500	670 (1600 mA g^{-1})	17
MoS_2-3D graphene	Hydrothermal	1405.9	1022.3	997 (700)	~100	2000	688 (8 A g^{-1})	18

Material	Synthesis method	First discharge capacity (mAh g^{-1})	First charge capacity (mAh g^{-1})	Capacity after (n) cycles (mAh g^{-1})	Coulombic efficiency %	Current density (mAh g^{-1})	Rate capability (mAh g-1) at (X) current density	Ref.
MoS_2-PPY-rGO	Wet reaction	1428	1085	1070 (400)	~100	200	~600 (2 A g^{-1})	19
MoS_2-graphene	Thermal reaction	1000	750	~1040 (120)	>97	100	460 (5 A g^{-1})	20
MoS_2/graphene	Hydrothermal	1160	896	1077 (150)	—	100	890 (1000 mA g^{-1})	21

*-indicates a value estimated from a published graph.

Table S3. Values of R_s, R_f, and R_{ct} of MoS_2/C electrodes obtained by fitting data according to the equivalent circuit model presented in Figure 7b.

	R_s (Ω)	R_f (Ω)	R_{ct} (Ω)
Initial	47.92	—	210.6
100th cycle	43.6	37.07	95.81

References

1. H. Hwang, H. Kim and J. Cho, *Nano Lett.*, 2011, **11**, 4826-4830.
2. K. Chang and W. Chen, *ACS Nano*, 2011, **5**, 4720-4728.
3. Y. T. Liu, X. D. Zhu, Z. Q. Duan and X. M. Xie, *Chem. Commun.*, 2013, **49**, 10305-10307.
4. Z. Wang, T. Chen, W. Chen, K. Chang, L. Ma, G. Huang, D. Chen and J. Y. Lee, *J. Mater. Chem. A*, 2013, **1**, 2202-2210.
5. G. Huang, T. Chen, W. Chen, Z. Wang, K. Chang, L. Ma, F. Huang, D. Chen and J. Y. Lee, *Small*, 2013, **9**, 3693-3703.
6. X. Cao, Y. Shi, W. Shi, X. Rui, Q. Yan, J. Kong and H. Zhang, *Small*, 2013, **9**, 3433-3438.
7. X. Zhou, L. J. Wan and Y. G. Guo, *Chem. Commun.*, 2013, **49**, 1838-1840.
8. L. Ma, G. Huang, W. Chen, Z. Wang, J. Ye, H. Li, D. Chen and J. Y. Lee, *J. Power Sources*, 2014, **264**, 262-271.
9. X. Zhou, Z. Wang, W. Chen, L. Ma, D. Chen and J. Y. Lee, *J. Power Sources*, 2014, **251**, 264-268.
10. Y. Gong, S. Yang, L. Zhan, L. Ma, R. Vajtai and P. M. Ajayan, *Adv. Funct. Mater.*, 2014, **24**, 125-130.
11. W. Fu, F. H. Du, J. Su, X. H. Li, X. Wei, T. N. Ye, K. X. Wang and J. S. Chen, *Sci. Rep.*, 2014, **4**, 4673.
12. Y. Liu, Y. Zhao, L. Jiao and J. Chen, *J. Mater. Chem. A*, 2014, **2**, 13109-13115.
13. J. Zhou, J. Qin, X. Zhang, C. Shi, E. Liu, J. Li, N. Zhao and C. He, *ACS Nano*, 2015, **9**, 3837-3848.
14. S. Han, Y. Zhao, Y. Tang, F. Tan, Y. Huang, X. Feng and D. Wu, *Carbon*, 2015, **81**, 203-209.
15. J. Wang, J. Liu, J. Luo, P. Liang, D. Chao, L. Lai, J. Lin and Z. Shen, *J. Mater. Chem. A*, 2015, **3**, 17534-17543.
16. H. Li, K. Yu, H. Fu, B. Guo, X. Lei and Z. Zhu, *J. Phys. Chem. C*, 2015, **119**, 7959-7968.
17. H. Yoo, A. P. Tiwari, J. Lee, D. Kim, J. H. Park and H. Lee, *Nanoscale*, 2015, **7**, 3404-3409.
18. F. Zhang, Y. Tang, H. Liu, H. Ji, C. Jiang, J. Zhang, X. Zhang and C. S. Lee, *ACS Appl. Mater. Interfaces*, 2016, **8**, 4691-4699.
19. D. Xie, D. H. Wang, W. J. Tang, X. H. Xia, Y. J. Zhang, X. L. Wang, C. D. Gu and J. P. Tu, *J. Power Sources*, 2016, **307**, 510-518.

20. C. Zhao, X. Wang, J. Kong, J. M. Ang, P. S. Lee, Z. Liu and X. Lu, *ACS Appl. Mater. Interfaces*, 2016, **8**, 2372-2379.
21. Y. Teng, H. Zhao, Z. Zhang, Z. Li, Q. Xia, Y. Zhang, L. Zhao, X. Du, Z. Du, P. Lv and K. Swierczek, *ACS Nano*, 2016, **10**, 8526-8535.